



Bioimprint aided cell recognition and depletion of human leukemic HL60 cells from peripheral blood

Received 00th January 20xx,
Accepted 00th January 20xx

DOI: 10.1039/x0xx00000x

rsc.li/materials-b

Anupam A.K. Das,^a Jevan Medlock,^a He Liang,^a Dieter Nees,^b David J. Allsup,^c Leigh A. Madden^d and Vesselin N. Paunov^{*a}

We report a large scale preparation of bioimprints of layers of cultured human leukemic HL60 cells which can perform cell shape and size recognition from a mixture with peripheral blood mononuclear cells (PBMCs). We demonstrate that the bioimprint-cell attraction combined with surface modification and flow rate control allows depletion of the HL60 cells from peripheral blood which can be used for development of alternative therapies of acute myeloid leukaemia (AML).

AML is a clonal malignant proliferation of transformed, bone-marrow derived myeloid precursors. The disease is characterised by the rapid proliferation of the neoplastic cells (myeloblasts) resulting in failure of normal haematopoiesis with consequential bone marrow failure rapidly resulting in death if untreated.¹⁻³ In the UK, overall survival is 16% 5 years from diagnosis. The prognosis is significantly worse in the elderly which is especially relevant as the majority of patients present over the age of 60 years.^{1,4-7} Therapy relies on 2–3 cycles of myeloablative chemotherapy followed by allogeneic stem cell transplant for a relatively small number of fit patients with poor prognostic features.⁸⁻⁹ This is accompanied with significant discomfort, long therapy for AML also is associated with prolonged inpatient stays, considerable morbidity related to anaemia, sepsis and bleeding and an attributable mortality of 5–10%. The majority of patients relapse following induction of chemotherapy for AML and subsequent therapy is associated with a low probability of success. Outcomes for AML patients have improved marginally over the past few decades, largely due to improvements in supportive care rather than dramatic improvements in the chemotherapeutic regimens efficacy.¹⁰ Bioimprinting is a promising area of materials chemistry aimed to mimic and exploit the lock-and-key interactions seen ubiquitously in nature.¹¹⁻¹⁴

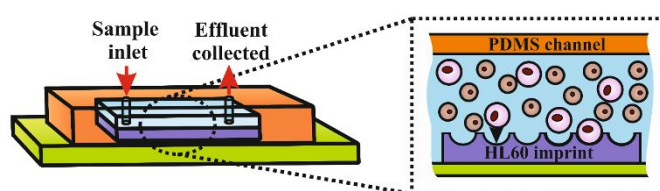


Figure 1. Schematic representation of the method of action of the flow through bioimprint chip for depletion of myeloblasts from peripheral blood.

Cell recognition systems are relatively cheap and simple to produce with few stipulations on storage and shelf life when compared with biological interventions. The scope for possible targets is also much greater, being able to target polysaccharides, enzymes, aptamers, DNA sequences, antibodies and whole cells.^{12,15,16,21-24} Bioimprints of whole cells were first reported by Dickert *et al.*¹⁷ who imprinted yeast into a sol-gel matrix. When incubated with several strains of yeast, the substrates showed a high affinity to the template material. This effect was attributed to the large contact surface areas between cells and the imprinted cavities. Other cell bioimprinting studies have progressed to cover a range of micro-organisms and human cells. Hayden *et al.*¹⁸ functionalised polyurethane with erythrocyte imprints, capable of discriminating between ABO blood groups. Though all cell targets possessed the same geometrical size and shape, imprints were able to discriminate on account of varied surface antigen expression. Subsequent studies were further able to discriminate cells with identical antibodies in different quantities to separate blood groups A1 and A2.¹⁹ Recent cell bioimprint studies largely focus on biosensor applications^{20,26} and are hindered by the small overall size of imprinted areas that can be produced which limits their applications for large scale extraction of targeted cell from cell mixtures. This research area is undergoing a rapid expansion towards using molecularly imprinted polymers as receptor mimics for selective cell recognition and sensing, a recent review of size and shape targeting of cancer found no evidence so far of the use of cancer bioimprints in a therapeutic setting.¹¹

^a Department of Chemistry and Biochemistry, University of Hull, Hull, HU67RX, UK.

^b Joanneum Research FmbH, Leonhardstrasse 59, 8010 Graz, Austria.

^c Hull York Medical School, University of Hull, University of Hull, Hull, HU67RX, UK.

^d Department of Biomedical Sciences, University of Hull, Hull, HU67RX, UK.

*Corresponding author: V.N.Paunov@hull.ac.uk, Tel: +44 1482 465660.

♣ Electronic Supplementary Information (ESI) available: See DOI: 10.1039/x0xx00000x

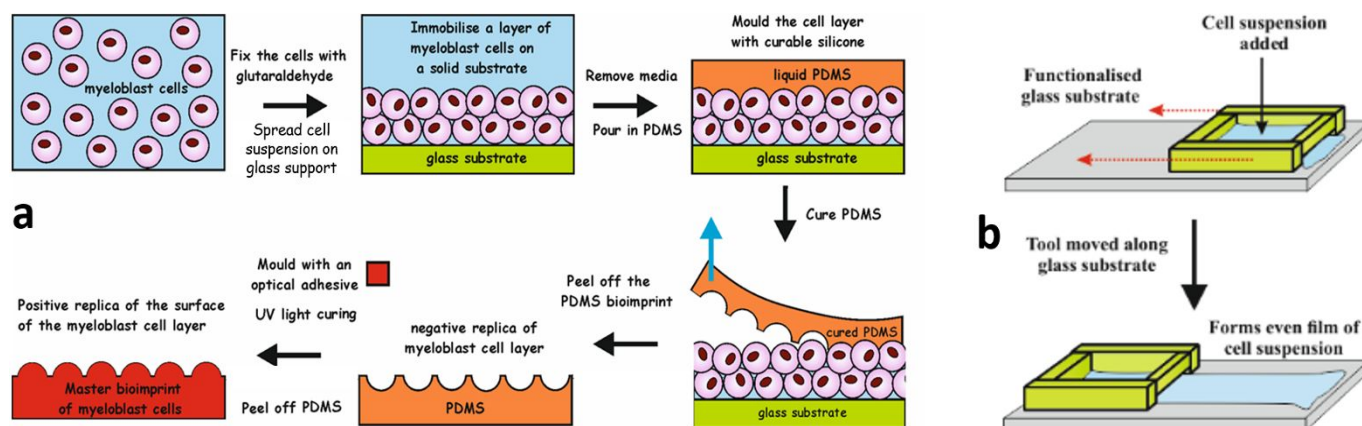


Figure 2 Schematic showing the preparation of negative and positive bioimprints from myeloblast cell layers by subsequent templating with curable silicone (PDMS) and photo-curable polyurethane (PU) resin, respectively. (b) Schematics showing our tool for spreading the HL60 cells aqueous suspension on glass to yield a uniform cell layer of large area.

Here we utilised for the first time AML cell bioimprints on a large scale as a vehicle to selectively target AML myeloblasts due to the inherent size and morphological discrepancies with normal peripheral blood mononuclear cells (PBMCs) (see Figure S1, ESI[†]). We explore AML bioimprinting as a new method for depletion of myeloblasts from peripheral blood cells by introducing selectivity via bespoke cell size and shape discrimination aided by myeloblast-bioimprint interactions. Our idea is based on incorporating AML myeloblast-imprinted substrates into a flow-through type of device which offers an alternative method for removal of the leukemic burden directly from patient aspirate. Successful leukaphoresis can potentially be used more frequently in the extraction of myeloblasts from peripheral blood which is critical in stabilizing AML patients with leukostasis associated with hyperleucocytosis. By reducing the number of circulating tumour cells, the likelihood of early relapse is also diminished.²⁵

HL60, an immortalized leukemic cell line derived from an AML patient, was used as a very good proxy for primary (patient derived) myeloblast cells throughout our study due to their availability and ease of culture. Here we show how the desired HL60 cell bioimprints were produced from HL60 cell layers. We also discuss the integration of the produced myeloblast imprint in a PDMS-based flow-through cell, in which its selectivity towards HL60 cells over the PBMCs is investigated (Figure 1). We fabricated bioimprints by impressing a layer of cultured HL60 myeloblasts with a curable polymer, which captures information for the cells shape, size and morphology. These were further casted with another polymer to create a “positive imprint” whose surface matches the original cell layer. Using roll-to-roll printing from the positive replica we produced a very large area of HL60 cell imprints. We engineered the surface of the bioimprint to have a weak attraction with the cells, which is strongly amplified when there is a shape and size match between the individual cells and the imprinted surface. Due to inherent size and morphology differences between myeloblasts and normal blood cells, this resulted in much higher retention of the former on the bioimprint. This allows their selective

trapping from peripheral blood based on cell shape and size recognition, much cheaper than using surface functionalisation with a combination of specific antibodies for myeloblasts. We tested the bioimprints selectivity in a device for depleting cultured HL60 cells from healthy white blood cells. This cell recognition technology can potentially deplete myeloblasts from the blood of AML patients and provide an alternative route for reducing the counts of the minimal residual disease, which is associated with reduced relapses and improved patient outcomes.

Cell handling. All live cell cultures and handling were carried out aseptically in a biosafety cabinet class II with laminar flow (Thermo Scientific). The HL60 cell line (Public Health England, cat. 98070106) was used as a surrogate myeloblast throughout the study. These were cultured aseptically in Roswell Park Memorial Institute Medium (RPMI) 1640 (Gibco), containing 10 vol% foetal bovine serum (Gibco), 5 mL penicillin and 5 mL streptomycin solutions at 37°C with 5% CO₂. Primary peripheral blood mononuclear cells (PBMCs) were obtained from anonymous healthy donors via the NHS blood transfusion service (under IRAS 214660) and stored in liquid nitrogen prior to use. The cells were slowly defrosted and washed 3 times in phosphate buffer saline solution (PBS, from Sigma-Aldrich). Removal of platelets contamination was achieved by centrifugation at 120g for 10 min and resuspension in PBS, repeated three times. Cell fixation was carried for both HL60 and PBMCs (at concentration 10⁷ cells ml⁻¹) by dropwise addition of the cell suspension to a stirred 0.5 v/v% glutaraldehyde (Sigma-Aldrich) in PBS solution. After 20 min., cells were washed by centrifugation at 400g for 4 min and re-suspended in PBS. All fixed cells were washed three times with PBS and stored at 4 °C until further use.

Bioimprint fabrication. The detailed schematic showing the production of the negative PDMS and positive PU based master HL60 myeloblast bioimprint is shown in Figure 2a.

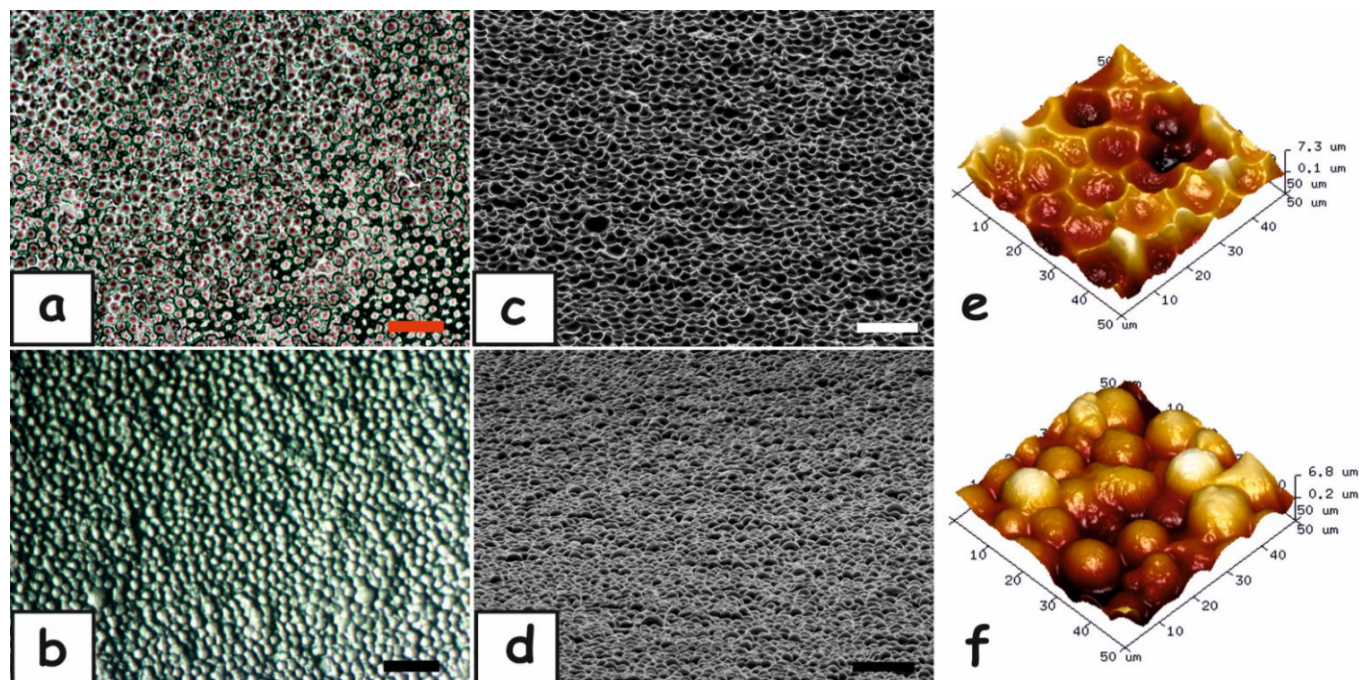


Figure 3. Bright field microscope images of (a) negative and (b) positive HL60 bioimprints, scanning electron microscopy images of (c) negative and (d) positive HL60 bioimprints and atomic force microscopy images (e) negative and (f) positive HL60 bioimprints. All Scale bars are 50 μm .

Glass substrates (70 cm \times 40 cm) were cleaned with acetone and 10% KOH (Sigma Aldrich) in ethanol for 1 h, rinsed with deionized water and treated with 20 wt% v/v poly(diallyldimethylammonium chloride) (PDAC) aqueous solution for 30 min. The substrates were further cleaned with deionized water and dried using compressed air. A sample of glutaraldehyde-fixed HL60 cells (6 g wet weight) and glucose (2.5 g) was mixed together in 30 mL of 0.1% (w/v) % xanthan gum solution. Spreading of this HL60 cell suspension on the glass substrate was done using a bespoke glass tool comprised of a square frame made of four glass strips, one of which was offset by 100 μm to create a gap. Figure 1b shows for the design and method of action of the spreading tool. The HL60 cell suspension was added to the frame interior and the device was moved along the glass substrate in one continuous motion in the direction opposite to the higher side, allowing an aqueous film of cell suspension (40 cm \times 70 cm) of uniform thickness (\sim 100 μm) to be deposited (Figure S2a, ESI[†]). The aqueous film was allowed to evaporate to a semi-dry state at room temperature, done in a laminar flow cabinet to reduce any contamination (Figure S2b, ESI[†]). Curable PDMS was made mixed at a 10:1 ratio of Sylgard 184 elastomer to accelerator and degassed by centrifugation (4000g, 10 min). A metal frame (interior space 65 \times 30 \times 4 cm) was added around the deposited cell smear and the PDMS (900 mL) poured evenly inside. To provide structural support, a polyester fabric sheet (Boyes UK, dimensions 65 \times 30 \times 0.1 cm) was added on top of the PDMS layer and allowed to cure at room temperature for 48 h (Figure S2c, ESI[†]). Cured PDMS bioimprints were removed from the glass surface and washed using warm water, detergent, ethanol and

finally deionized water and then dried using compressed air. The negative PDMS based bioimprint (Figure S2d, ESI[†]) was then copied onto a transparent polyethylene terephthalate (PET) foil with a pre-deposited layer of photo-curable PU-acrylic resin (supplied from Joanneum Research FmbH, Graz, Austria) under three 365 nm 10W portable UV lamps for 10 min (Figure S2e, ESI[†]) to produce a positive bioimprint (Figure S2f, ESI[†]). Multiple copies of positive HL60 bioimprints (62.9cm \times 25cm shims) were made using the aforementioned process.

Replication of bioimprints by Roll-to-Roll (R2R) printing. Roll-to-Roll nanoimprinting from sim made of the positive PU-acrylic resin on PET bioimprint shim was carried out by using Nano-Imprinting Lithography (R2R NIL) in collaboration with Joanneum Research FmbH. Herein, the positive shim imprint (60cm \times 25cm) was mounted to the circumference of the imprinting shim of the R2R NIL printer where it was rolled and pressed against an incoming PET foil pre-coated with a film of UV curable acrylic resin and simultaneously cured by UV light in real time.²⁷ R2R NIL printing was done at a rate of 1 m s⁻¹ for a user defined length (see more detail in Figure S3, ESI[†]) to produce acrylic-resin-based negative imprints of myeloblast layers on clear PET foil of 20 cm width. The R2R NIL replication yielded negative HL60 bioimprints, typically with a length of several hundred metres, before any visible erosion of the master positive imprint was detected.

Bioimprint surface modification. The negative HL60 bioimprints replicated on a large scale via R2R nanoimprinting on PET foil were further surface functionalised to incur a weak attraction between target myeloblasts and bioimprints.

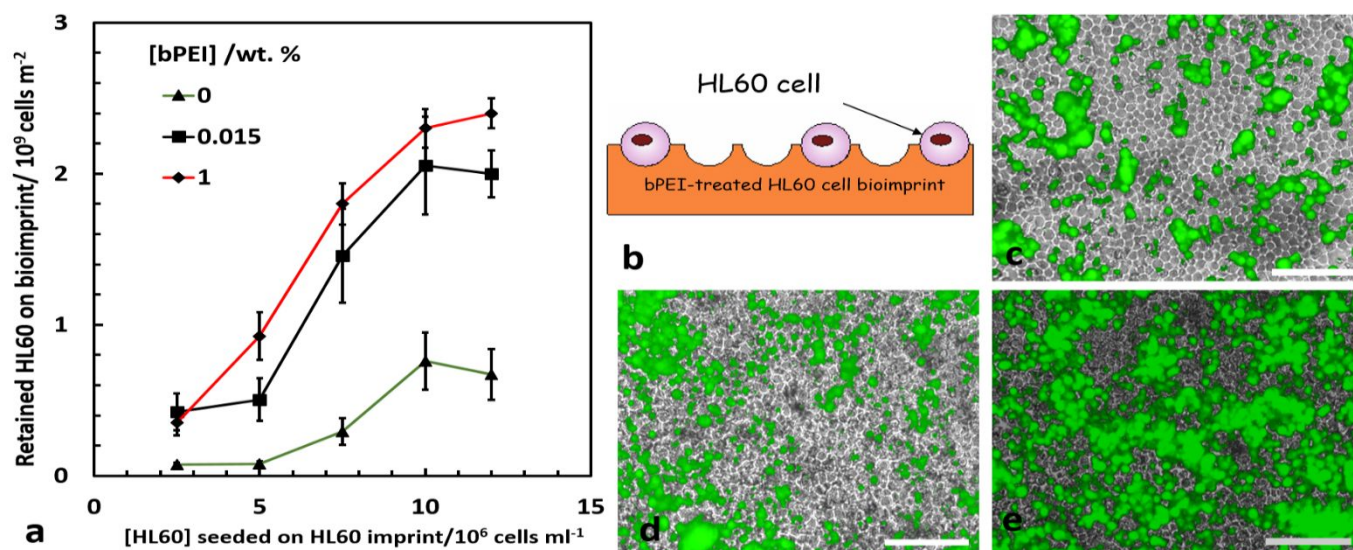


Figure 4 (a) Graph showing the retention of the HL60 cells on HL60 bioimprints pre-treated with different concentration of bPEI followed by treatment with 1 wt% P407. (b) Schematic showing the trapping of HL60 cells on the HL60 imprint. Optical and overlapped fluorescence microscope image of imprints containing (c) 5 million, (d) 7.5 million and (e) 10 million HL60 cells mL⁻¹. The bioimprint becomes saturated above 10 million HL60 cells mL⁻¹. All Scale bars are 100 μ m.

The imprints were first exposed to oxygen plasma (Harrick Plasma PDC 32G) at 147 Pa, using an RF power of 16 W for 4 min. The plasma treated imprint was further layered using a glass rod with branched polyethylene imine (bPEI) – see ESI for more details. The imprint was incubated with bPEI solution for 20 min, then submerged in deionized water, gently stirred for 5 min, then rinsed with deionised water and dried in air stream.

HL60 cells/PBMCs fluorescence staining. The fixed cells were fluorescently labelled to allow numeration and identification of the type of cells retained on the HL60 negative bioimprints. HL60 cells were stained by dropwise addition of 100 μ L of 0.025% (w/v) 1,2-dioleoyl-sn-glycero-3-phosphoethanolamine N(carboxyfluorescein) in ethanol. PBMCs were stained via a similar method using 1,2-dioleoyl-sn-glycero-3-phosphoethanolamine-N (lissamine rhodamine B sulphonyl) (ammonium salt). The excess dye was removed by multiple washing and replacing the media with PBS using centrifugation at 400g for 5 min. An Olympus BX51 microscope coupled with a mercury lamp excitation source and DP70 camera (Olympus) with ImageProPlus software was used to capture images of the captured cell populations retained on the HL60 bioimprint.

Flow-through bioimprint chip fabrication. The bPEI-treated bioimprints were incorporated into flow-through chips made from a glass slide and a moulded PDMS channel. PDMS strips (3 \times 6 \times 1 cm) were made yielding an exposed channel (0.5 \times 4 \times 0.1 cm) which was punctured to allow inlet and outlet tubing to be fed (internal diameter 1 mm). The PDMS substrate and a clean glass microscope slide were treated in oxygen plasma (32 W, 147 Pa) for 3 min. A stripe of the surface functionalised bioimprint (0.5cm \times 4 cm) was trapped between the activated glass slide and covered with pre-fabricated PDMS block, with the bioimprint fixed in the moulded channel. The schematic of the flow chip is shown in Figure 1 and the photographs of the produced PDMS based chips are shown in Figures S4a and S4b,

ESI*. The chip was clamped to ensure a tight seal and cured at 40 $^{\circ}$ C for 30 min to bind the glass to the PDMS block. The chip with the embedded HL60 bioimprint was loaded with 200 μ L of 1% or 3% (w/v) aqueous solution of Poloxamer 407 (Sigma-Aldrich) and incubated for 20 mins prior to the cell-selectivity experiments. This was done to reduce the non-specific cell adhesion on the PDMS channel, the bioimprint and the tubing. Syringe pump was used to pre-wash the chips, passing 10 mL of PBS through the chip at a rate of 225 mL/h.

HL60 and PBMCs cell retention experiments. Retention of fixed HL60 cells was investigated as a function of the HL60 cell concentration seeded over the imprint for a range of substrate functionalization parameters. Suspensions of fluorescently tagged, fixed HL60 cells in PBS (100 μ L) were made at a range of concentrations. Cell samples were injected into flow-through chips containing the surface treated HL60 negative bioimprints and incubated for 1 h. Inlet and outlet tubing (internal diameter 1 mm) were fitted to opposite ends of the chamber containing the bioimprint. Unbound cells were washed off the bioimprint using a syringe pump by elution with 10 mL PBS at a fixed flow rate. Retention of HL60 cells was assessed by using a combination of bright field and fluorescence microscopy at various sites across the bioimprint (20 fields of view). The static condition experiment is shown in Figure 1. Cells were numerated by using fluorescence microscope images collected using both FITC filter set (showing HL60 as green) and TRITC filter sets (showing PBMCs as red) in order to separately assess each cell type collected on the bioimprint. To separate conjoined cells, the watershed feature was used in ImageJ. A lower boundary of cell size was used to prevent fluorescent cell fragments and debris from being counted as a whole cell, this was found from analysis of fluorescently tagged cell populations. Results were compared as the average number of cells per metre squared, hereafter termed the cell area density.

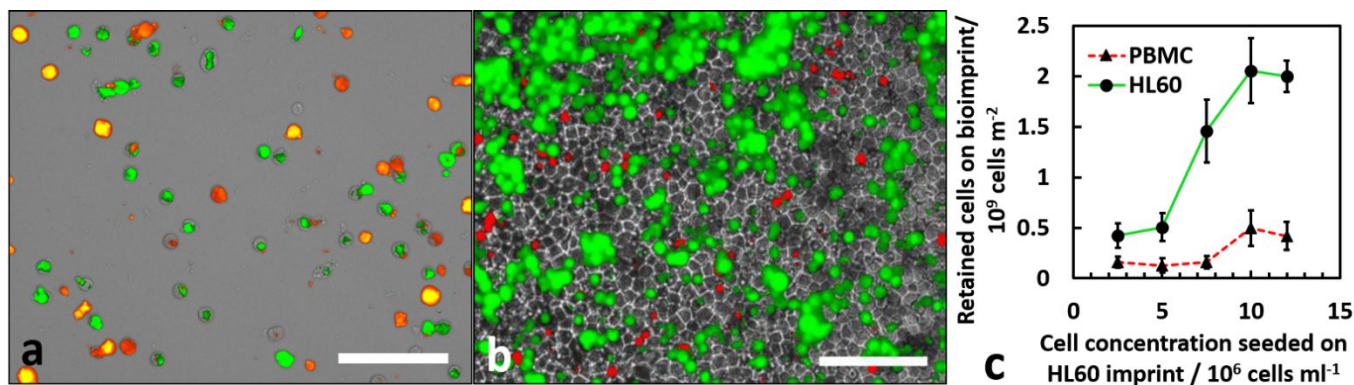


Figure 5. Bright field with fluorescence overlapped microscope images (a) showing the retention of the HL60 (green) and PBMC (red) cells on an un-imprinted flat PU-coated slide and (b) on bioimprint functionalised with 0.015 wt % bPEI and 1 wt% Poloxamer 407. (c) The retention of the HL60 and PBMCs on the bioimprint vs cell seeding concentration.

The Image J macro used for this function is enclosed in the ESI[†]. AML poses a difficult target for conventional biological assays owing to a heterogeneous antigen expression and sheer abundance of neoplastic material. However, the fluid nature of the malignancy and size discrepancy between healthy and cancerous tissue was targeted by a bioimprint. The size differences can be seen in Figure S1a and S1b, ESI[†] showing live bright field optical microscopy images of a sample of typical HL60 cells and PBMCs. Flow cytometry data show that the HL60 cells are $\sim 47\%$ larger than the average size of the PBMCs, i.e. there is a large size disparity between PBMCs and HL60 cells. All cells were chemically fixated using glutaraldehyde prior to use to prevent deformation and damage during the imprinting process. For consistency we did the selectivity experiments with the same batches of fixed cells. The bright field microscopy images of glutaraldehyde fixed HL60 cells and PBMCs is shown in Figures S1c and S1d, showed similar surface morphology and cell shape information. Optical microscopy image of the negative PDMS-based HL60 cell imprint, copied directly from the HL60 cell layer, is shown in Figure 3a, while the positive PU-based replica is represented by Figure 3b, 3d and 3f with bright field, SEM and AFM images, respectively. SEM and AFM images of the resultant negative PU-based HL60 bioimprint produced by replicating of the positive shim and used for trapping the HL60 cells in the microfluidic device are shown in Figure 3c and 3e, respectively. These samples of bioimprints were produced with the NIL R2R printing according to the procedure described above. Further surface treatment of the negative HL60 bioimprint was aimed to introduce a weak attraction between the imprint and the negatively charged HL60 cells. This was achieved by additional surface treatment of the produced imprint on PET foil by oxygen plasma which oxidizes the resin surface and creates carboxyl surface groups which serve as adsorption sites for the subsequent treatment with a cationic polyelectrolyte (bPEI), whose adsorption makes the bioimprint surface cationic. The cell surfaces are normally negatively charged due to the presence of COOH groups from carbohydrates and glycoproteins on their cell membranes.²⁸ As the adhesion force of the cells to the bioimprint depends on the contact area between them, cells that better match the

imprinted cavities are stronger attached to its surface. Since PBMCs are much smaller than the HL60, the former would only interact with the imprint surface in a “point contact” which leaves them weakly bound. On the other hand, the HL60 cells better match the HL60 imprint cavities which leads to full contact between the imprint surface and a large portion of the HL60 outer cell membrane. Above certain specific flow rate, the flow in the chip would “flush off” the weakly bound PBMCs while the HL60 cells remain trapped on the imprint.

In order to increase the selectivity of the bioimprint and reduce non-specific binding of PBMCs on the imprint, the chip channels and the adjacent tubing, surfaces were further passivated with a Pluronic[™] surfactant (Poloxamer 407) which is a three-block co-polymer with one hydrophobic group in the middle (polypropylene oxide) and two on each side that are hydrophilic (polyethylene oxide). The Poloxamer 407 coating also minimizes the close contact between the cells and the bPEI coating. We tested several different concentrations of the cationic polyelectrolyte (bPEI), the Poloxamer 407 concentration and varied the flow rates in order to improve the bioimprint and chip selectivity with respect to retention of the HL60 cells. This was done in order to improve the bioimprint selectivity for HL60 compared to PBMCs where the cells mixture was incubated in the chip and later flushed with PBS at different flowrates.

Theoretical calculations have shown that the substantial increase of the area of contact between the cell imprint and a matching cell in the near vicinity can increase the energy of even a weak cell-surface attraction by several orders of magnitude.²⁴ We found that the retention of the HL60 cells on the imprint increased with the increase in the bPEI concentration used to pre-treat the HL60 cell bioimprint, as shown in Figure 4a. The resulting graph resembles an adsorption isotherm for these cells on the bioimprint surface at fixed flow rate, where the increase of HL60 seeding concentration leads to occupation of more surface cavities on the bioimprint (see Figure 4b). The number of HL60 cells captured on the HL60 imprint increases with the increase in their seeding concentration (see Figures 4c, 4d and 4e). The imprint was completely saturated above HL60 seeding concentration of 10^6 cells mL^{-1} .

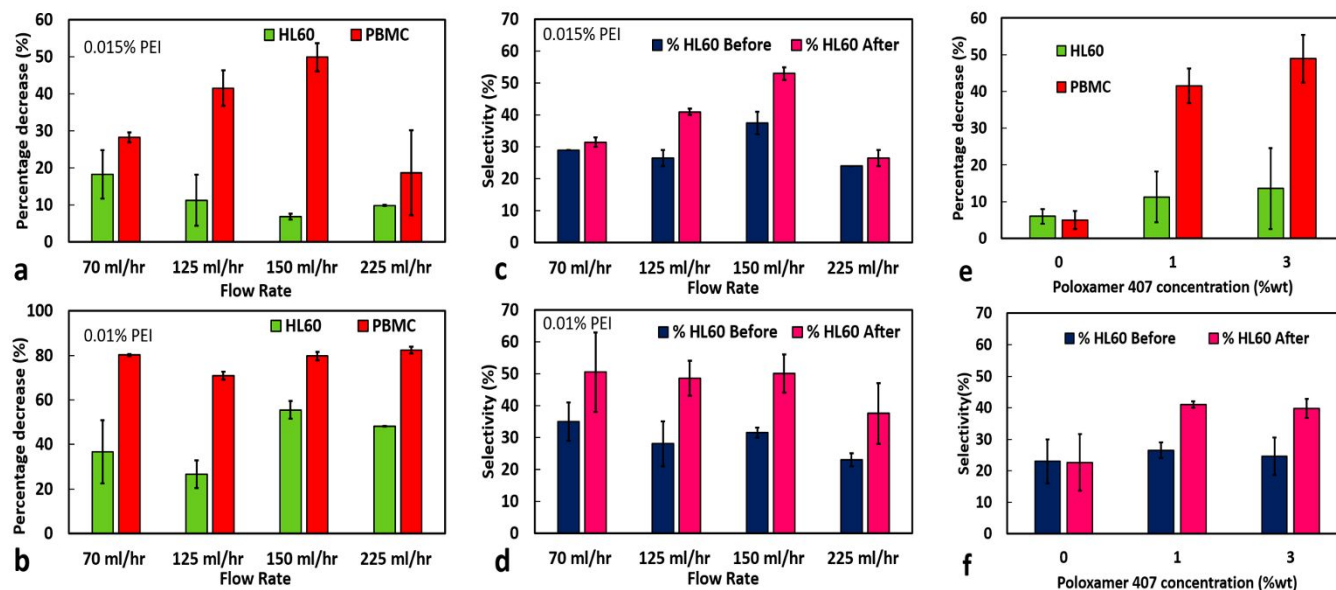


Figure 6. The percentage of decrease of the HL60 cells and PBMCs on the negative HL60 bioimprint after flushing the chip with PBS at different flowrates. The bioimprint was treated with (a) 0.015% and (b) 0.01 wt% bPEI with 1 wt% Poloxamer 407 functionalised and the corresponding HL60 selectivity of the bioimprint (in %) in (c) 0.015 wt% and (d) 0.01 wt% bPEI, respectively at the same conditions. (e) The percentage decrease of HL60 and PBMC after flushing at 150 ml/hr flowrate and (b) the selectivity of the HL60 imprint towards HL60 (in %) on imprints treated with 0.015% bPEI and functionalised by incubation with aqueous solutions of different concentrations of Poloxamer 407.

Note that the amount of retained HL60 cells at fixed flow rate depends on the cationic polyelectrolyte concentration used to pre-treat the bioimprint. However, we found that very low bPEI concentration (0.015 wt%) leads to almost full saturation and further increase does not significantly increase the retained HL60 amount (cf. Figure 4a at bPEI 1 wt%). It was also observed that the flat (non-patterned) PU surface has no selectivity compared to the HL60 bioimprint as shown in Figures 5a and 5b. The experiment was also conducted using PBMCs which showed minimum adhesion as evident from the curve in Figure 5c. In order to check the selectivity of the HL60 cells over the PBMCs for HL60 imprint, a model mixture of HL60 and PBMCs at fixed HL60:PBMCs ratio of 20:80 was prepared in PBS and incubated on the imprint pre-coated with desired amount of bPEI and pre-treated with Poloxamer 407. After 1 hour of incubation the chip was flushed with PBS at a range of flowrates. It was found that in both cases where the HL60 imprints were treated with 0.01 wt% and 0.015 wt% bPEI showed more efficient HL60 retention compared to PBMC as evident from Figures 6a and 6b, respectively at all flowrates ranging from 70 mL/h to 225 ml/h. The percentage decrease of HL60 and PBMC cell after flushing of the chip and the bioimprint selectivity with respect to HL60 cells are calculated as described in ESI†. The highest amount of HL60 compared to PBMC was retained in case of the imprints coated with the combination of 0.015 wt% bPEI, 1 wt% Poloxamer 407 and flushed with PBS at a flowrate of 150 ml/h as shown in Figure 6a. Among all the combinations tested it was found that imprint coated with 0.015 wt% PEI, 1 wt% Poloxamer 407 and flushed with PBS at a flowrate of 150 ml/h showed the largest selectivity potential and hence was used for further

experiments. These results were also reflected in Figures 6c and 6d where the percentage of HL60 increased compared to the PBMCs before and after flushing the chip with PBS. The effect of the Poloxamer 407 concentration was also evaluated on the imprint selectivity towards the HL60 cells. Without Poloxamer 407 treatment the imprint retained comparable amounts of PBMCs and HL60 as evident from Figures 6e and 6f due to strong non-specific adsorption at this flowrate. The additional coating of the imprint with 1% and 3% Poloxamer 407 in two different cases showed preferential HL60 retention (Figure 6e and 6f). Note that the PBMCs have much higher percentage of decrease on the imprint than the HL60 cells, which predominantly remain on the bioimprint after the flushing step. These results call for some discussion. The initial idea was to modify imprint surface to attract the negatively charged target cells (HL60). As the PBMCs are also negatively surface charged cells, it was important to have a weaker attraction for the PBMC compared to the HL60. This was done by cell shape and size recognition where the cell adhesion is amplified by substantial surface area of contact between the cells and the imprint.²⁴ The weak and relatively short-range attraction can be increased by several orders of magnitude by simply getting the surface area of contact maximized and selectively flushing out cells with smaller area of contact (PBMCs) compared to the larger HL60 which better fit the bioimprint cavities. The role of the Poloxamer 407 was to passivate the bioimprint surface and to slightly offset the minimal distance of approach of PBMCs, which would minimise the non-specific adhesion of these cells to the imprint and weaken their attachment. Although the Poloxamer 407 coating had the same effect on HL60 cells, their

larger contact area upon cell shape and size recognition by the matching imprint cavities yields much higher force of attachment which makes possible the discrimination between HL60 and PBMCs by the bioimprint.

In summary, we showed that bioimprints of cultured HL-60 cells, representative of patient derived myeloblasts can be produced efficiently using the process of casting cell layers with curable resins which copy part of the cell surface and retains information about their size, shape and surface morphology on the imprint. The cell imprint in curable silicone (PDMS) were subsequently copied onto a positive replica from UV-curable polyurethane (PU)-acrylic resin and reproduced on a very large scale using the Roll-to-Roll NIL printing. The negative HL60 bioimprints were then successfully integrated into a PDMS-based flow-through chip and tested to explore the HL60 retention capacity and selectivity in a mixture with PBMCs. It was found that these bioimprints do have a specificity for the HL60 cells when the surfaces were pre-treated with a cationic polyelectrolyte (bPEI) and Poloxamer 407. It was also concluded that Poloxamer 407 treatment improves the bioimprint selectivity towards HL60 cells. This bioimprint-based technology can be successfully upscaled and integrated into a medical device for depletion of residual myeloblasts from peripheral blood of AML patients before and after chemotherapy, with the aim of deepening the remission of treated patients and reducing minimal residual disease,²⁹ an endpoint associated with improved patient outcomes.

Acknowledgements

VNP, LAM and DJA acknowledge funding from CRUK for their Pioneer Award grant. JM thanks the University of Hull for funding his PhD studentship. HL, VNP, LAM and DJA also thank the University of Hull and the UK Higher Education Innovation Fund for the financial support of this study.

ORCID

Anupam Das: 0000-0003-1948-8811

Jevan Medlock: 0000-0003-2425-3777

He Liang: 0000-0002-7361-4690

David Allsup: 0000-0001-6159-6109

Leigh A. Madden: 0000-0002-1503-1147

Vesselin N. Paunov: 0000-0001-6878-1681

Conflicts of interest

There are no conflicts of interest to declare.

References

- C. O'Brien, E. S. Prideaux and T. Chevassut, *Adv. Hematol.*, 2014, **2014**, 103175.1-15.
- E. Estey and H. Döhner, *The Lancet*, 2006, **368**, 1894-1907.
- J.L. Shipley and J.N. Butera, *Exp. Hematol.*, 2009, **37**, 649-658.
- Y. Ofran, M.S. Tallman and J.M. Rowe, *Blood*, 2016, **128**, 488-96.
- D.A. Pollyea, H.E. Kohrt and B.C. Medeiros, *Brit. J. Haematol.*, 2011, **152**, 524-42.
- J.E. Kolitz, *Brit. J. Haematol.*, 2006, **134**, 555-572.
- J.M. Bennett, D. Catovsky M.-T. Daniel, G. Flandrin, D.A.G. Galton, H.R. Gralnick and C. Sultan, *Brit. J. Haematol.*, 1976, **33**, 451-458.
- A.K. Burnett, *Hematol. Amer. Soc. Hematol. Educ. Program*, 2012, **2012**, 1-6.
- C.S. Viele, *Semin. Oncol. Nurs.*, 2003, **19**, 98-108.
- H. Dombret and C. Gardin, *Blood*, 2016, **127**, 53-61.
- J. Medlock, A.A.K. Das, L.A. Madden, D.J. Allsup, V.N. Paunov, *Chem. Soc. Rev.*, 2017, **46**, 5110-5127.
- A.L. Bole and P. Manesiotis, *Adv. Mater.*, 2016, **28**, 5349-5366.
- Y. Ge and A.P. Turner, *Trends Biotechnol.*, 2008, **26**, 218-224.
- G. Vasapollo, R. Del Sole, L. Mergola, M.R. Lazzo, A. Scardino, S. Scorrano and G. Mele, *Int. J. Mol. Sci.*, 2011, **12**, 5908-5945.
- T.S. Bedwell and M.J. Whitcombe, *Anal. Bioanal. Chem.*, 2016, **408**, 1735-1751.
- S. Sacanna, W.T.M. Irvine, P.M. Chaikin and D.J. Pine, *Nature*, 2010, **464**, 575-578.
- F.L. Dickert and O. Hayden, *Analyt. Chem.*, 2002, **74**, 1302-1306.
- O. Hayden, K.J. Mann, S. Krassnig, F.L. Dickert, *Angew. Chem. Int. Ed. Engl.*, 2006, **45**, 2626-2629.
- A. Mujahid and F.L. Dickert, *Sensors*, 2015, **16**, 51.1-17.
- K. Eersels, B. van Grinsven, A. Ethirajan, S. Timmermans, K.L. Jiménez Monroy, J.F. Bogie, S. Punniyakoti, T. Vandenryt, J.J. Hendriks, T.J. Cleij, M.J. Daemen, V. Somers, W. De Ceuninck, P. Wagner, *ACS Appl. Mater. Interf.*, 2013, **5**, 7258-67.
- J. Borovicka, S.D. Stoyanov, V.N. Paunov, *Nanoscale*, 2013, **57**, 8560-8568.
- J. Borovicka, W.J. Metheringham, L.A. Madden, C.D. Walton, S.D. Stoyanov, V.N. Paunov, *J. Am. Chem. Soc.*, 2013, **135**, 5282-5285.
- J. Borovicka, S.D. Stoyanov, S.D., V.N. Paunov, *MRS Proceedings*, 2012, 1498, mrsf12-1498-110-06, doi:10.1557/opl.2013.14.
- J. Borovicka, S.D. Stoyanov, V.N. Paunov, *Phys. Rev. E.*, 2015, **92**, 032730.1.
- C.S. Hourigan and J.E. Karp, *Nat. Rev. Clin. Oncol.*, 2013, **10**, 460-471.
- J. Pan, W. Chen, Y. Mab and G. Pan., *Chem. Soc. Rev.*, 2018, **47**, 5574-5587.
- M. Leitgeb, D. Nees, S. Ruttloff, U. Palfinger, J. Götz, R. Liska, M.R. Belegatis, B. Stadlober, *ACS Nano*, 2016, **10**, 4926-4941.
- A.A.K. Das, R.F. Fakhruddin and V.N. Paunov, CHAPTER 9 Artificial Multicellular Assemblies from Cells Interfaced with Polymers and Nanomaterials, in *Cell Surface Engineering: Fabrication of Functional Nanoshells*. 2014, The Royal Society of Chemistry. p. 162-184.
- U. Platzbecker, J.M. Middeke, K. Sockel, R. Herbst, D. Wolf, C.D. Baldus, U. Oelschlägel, A. Mutherig, L. Fransecky, R. Noppeney, G. Bug, K. Götz, A. Krämer, T. Bochtler, M. Stelljes, C. Groth, A. Schubert, M. Mende, F. Stölzel, C. Borkmann, A.S. Kubasch, M. von Bonin, H. Serve, M. Hänel, U. Dührsen, J. Schetelig, C. Röllig, M. Kramer, G. Ehninger, M. Bornhäuser, C. Thiede, *Lancet Oncol.* 2018, **19**, 1668-1679.